Magnesium Technology 2013
Edited by: Norbert Hort, Suveen N. Mathaudhu, Neale R. Neelameggham, and Martyn Alderman
TMS (The Minerals, Metals & Materials Society), 2013

HIGH TEMPERATURE DEFORMATION OF MAGNESIUM ALLOY TX32-0.4Al-0.8Si

C. Dharmendra[1] , K.P. Rao[1] , N. Hort[2] , K.U. Kainer[2]

[1]Department of Mechanical and Biomedical Engineering
City University of Hong Kong, 83 Tat Chee Avenue, Kowloon, Hong Kong SAR
[2]Helmoltz-Zentrum Geesthacht, Max-Planck Str. 1, Geesthacht 21502, Germany

Keywords: Mg-Sn-Ca-Al-Si alloy, Hot deformation, Processing map, Kinetic analysis

Abstract

The effect of aluminum and silicon as micro-alloying elements in TX32 magnesium alloy on its hot deformation behavior has been studied by conducting uniaxial compression tests at various combinations of temperatures and strain rates in the ranges 300-500 °C and 0.0003-10 s^{-1}. A processing map has been developed and the effect of processing conditions on deformation behavior has been analyzed. Two processing windows that enable good hot working of the alloy are identified at (1) 390-500 °C/0.0003-0.005 s^{-1} (Domain 1), (2) 430-500 °C/0.3-10 s^{-1} (Domain 2). The kinetic analysis is obeyed in these two domains and the relevant apparent activation energy values are found to be 215 and 170 kJ/mole respectively. These are higher than that for self-diffusion in magnesium suggesting that intermetallic particles present in the matrix generate back stress.

Introduction

Magnesium alloys have become very attractive in applications such as automotive, aerospace and railway industries due to their light weight and high specific strength. In spite of having better mechanical properties than cast alloys, wrought Mg alloys still have limited applications due to their poor workability at lower temperatures [1,2] and their strong anisotropic character [3]. These limitations are due to their hexagonal close-packed (hcp) crystal structure and therefore insufficient number of slip systems [1,2]. At room temperature, basal slip is the principal slip system. Due to the temperature dependency of critical resolved shear stress of other slip systems, non-basal slip systems such as prismatic and pyramidal are activated at higher temperatures only [4,5]. Magnesium develops pronounced crystallographic textures after deformation operations which is not desirable for further processing [6]. In practice, formability can be improved by working at higher temperatures, alloying additions and finer grain sizes [7]. All of these can be rationalized in terms of non-basal slip activation [8].

Mg-Sn-Ca (TX series) alloys are new magnesium wrought alloys that are designed to offer good corrosion and creep resistance [9]. Among them, Mg-3Sn-2Ca (TX32) alloy is identified as the most promising one as it exhibited good creep resistance [9,10]. The addition of aluminum and silicon at micro-alloying levels are considered to further enhance the properties of this alloy. Aluminum improves room temperature mechanical properties of Mg by solid solution strengthening [11] due to large atomic size difference (16%) while silicon forms intermetallic particles which can enhance creep strength.

The aim of this work is to evaluate the hot workability of TX32-0.4Al-0.8Si alloy in as-cast condition by applying kinetic analysis and developing a processing map using flow stress data obtained in compression tests. The standard kinetic rate equation relating the strain rate ($\dot{\varepsilon}$) and temperature (T) to the steady state flow stress (σ) is given by [12]:

$$\dot{\varepsilon} = A\sigma^n \exp\left[-\frac{Q}{RT}\right] \quad (1)$$

where A = constant, n = stress exponent, Q = activation energy, and R = gas constant. The rate-controlling mechanisms are identified on the basis of the activation parameters n and Q. The technique of processing maps is based on the dynamic materials model [13,14]. The efficiency of power dissipation occurring through microstructural changes during deformation is given by:

$$\eta = 2m/(m+1) \quad (2)$$

where m is the strain rate sensitivity of flow stress. Further, the extremum principles of irreversible thermodynamics as applied to continuum mechanics of large plastic flow [15] have been explored to define a criterion for the onset of flow instability given by:

$$\xi(\dot{\varepsilon}) = \frac{\partial \ln[m/(m+1]}{\partial \ln \dot{\varepsilon}} + m \leq 0 \quad (3)$$

These equations can be employed to find out the effect of temperature and strain rate on deformation processing and microstructural evolution.

Experimental Details

Mg – 3 wt.% Sn – 2 wt.% Ca – 0.4 wt.% Al-0.8 wt.% Si (TX32 – 0.4Al-0.8Si) alloy was prepared using 99.99% pure Mg, 99.96% pure Sn, 98.5% pure Ca, 99.9% Al and 99.9% Si. The alloy was molten at about 720 °C under a protective cover of Ar+3% SF_6 mixed gas atmosphere, and was poured into pre-heated permanent molds to obtain cylindrical billets of 100 mm diameter and 350 mm length. For compression testing, cylindrical specimens of 10 mm diameter and 15 mm height were machined from the as-cast billet. A 1 mm diameter hole was drilled at mid height of the specimen for inserting a thermocouple to measure the specimen temperature as well as the adiabatic temperature rise during the compression test.

The compression tests in the temperature range 25-250 °C were conducted at a low strain rate of 0.0001s^{-1} using a computer-controlled servo-hydraulic testing machine to evaluate strength of the alloy. The data for developing processing maps were obtained from uniaxial compression tests conducted at constant true strain rates in the range 0.0003 – 10 s^{-1} and temperature range 300 – 500 °C. Details of the test set-up and procedure are described in an earlier publication [16]. Constant true strain rate during a test was achieved using an exponential decay of actuator speed in the servo hydraulic machine. Graphite powder mixed with grease was used as the lubricant in all the experiments. The specimens were

deformed up to a true strain of about 1.0 and then quenched in water. The load - stroke data were converted into true stress - true strain curves using standard equations. The flow stress values were corrected for the adiabatic temperature rise. The deformed specimens were sectioned in the center parallel to the compression axis and the cut surface was mounted, polished and etched for metallographic examination.

Results and Discussion

The initial microstructure of as-cast TX32-0.4Al-0.8Si alloy is shown in Figure 1(a). The average grain diameter was about 300 μm. The intermetallic particles are identified as CaMgSi and Ca_2Sn phases based on X-ray diffraction (XRD) and electron probe micro analysis (EPMA), and are marked in the scanning electron micrograph as shown in Figure 1(b).

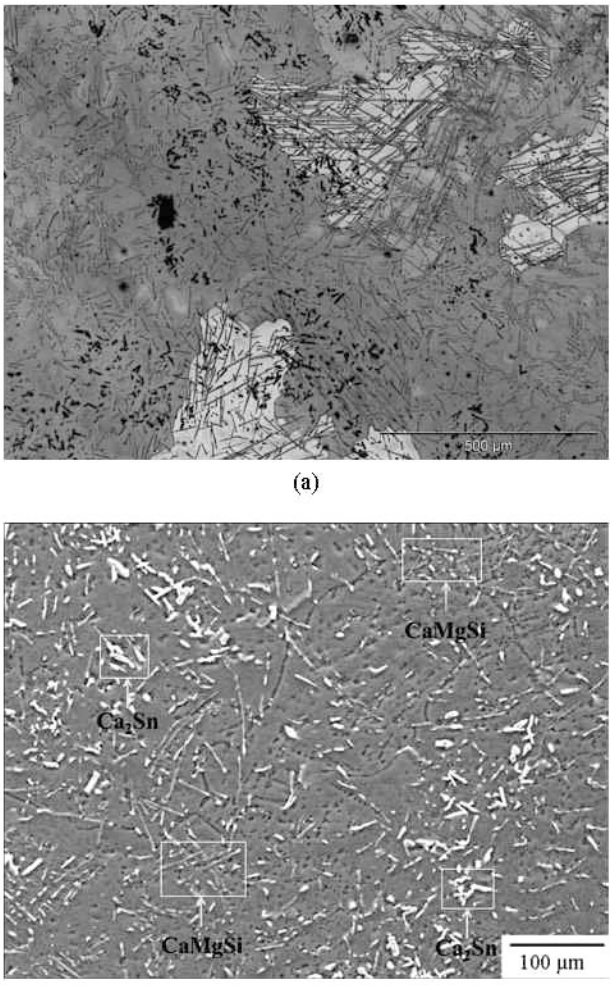

Figure 1. (a) Optical and (b) Scanning electron micrographs of TX32-0.4Al-0.8Si alloy, the latter showing CaMgSi and Ca_2Sn phase particles.

The variation of the ultimate compressive strength with temperature in the range 25 – 250 °C at a strain rate of $0.0001s^{-1}$ obtained from compression tests of TX32-0.4Al-0.8Si alloy is shown in Figure 2. A strain rate slower than that used for generating processing maps is selected for obtaining the strength of the alloy in this temperature range. Figure 2 shows that the strength drops continuously with increase in temperature. The values for the alloy Mg-3Sn-2Ca-0.4Al (with-out Si addition) are also plotted in this figure for the purpose of comparison and to evaluate the effect of Si. The reduction in strength with Si addition may be attributed to the presence of CaMgSi intermetallic particles. The Si addition often promotes the precipitation of Si-containing particles which form during solidification and are quite detrimental to the mechanical properties of Mg alloys [17, 18]. Asl et al. [11] have indicated that addition of Si to some aluminum containing magnesium alloys improves creep resistance while reducing the room temperature mechanical properties. The role of Si on mechanical and creep properties of such alloy systems is not fully understood. The present results, however, clearly show that 0.8% Si addition is not useful for improving the strength of the TX32 base alloy containing 0.4%Al.

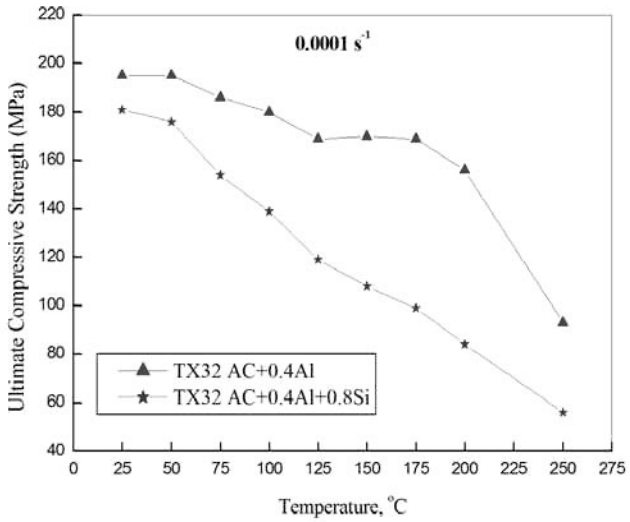

Figure 2. Variation of ultimate compressive strength (UCS) values with temperature for TX32-0.4Al and TX32-0.4Al-0.8Si alloys.

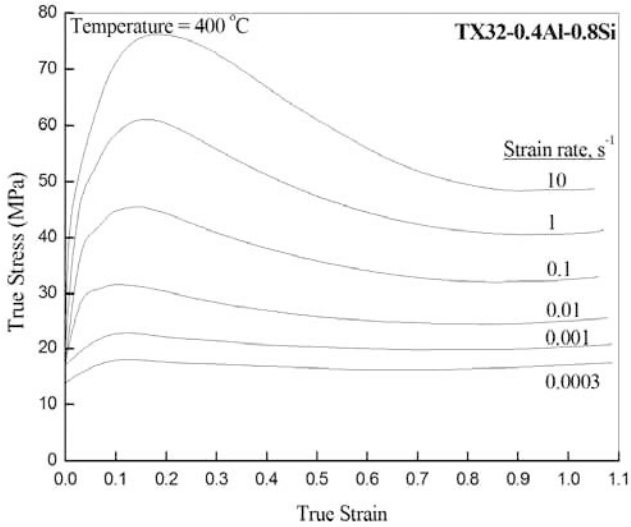

Figure 3. True stress - true strain curves obtained at 400 °C on TX32-0.4Al-0.8Si alloy in compression at different strain rates.

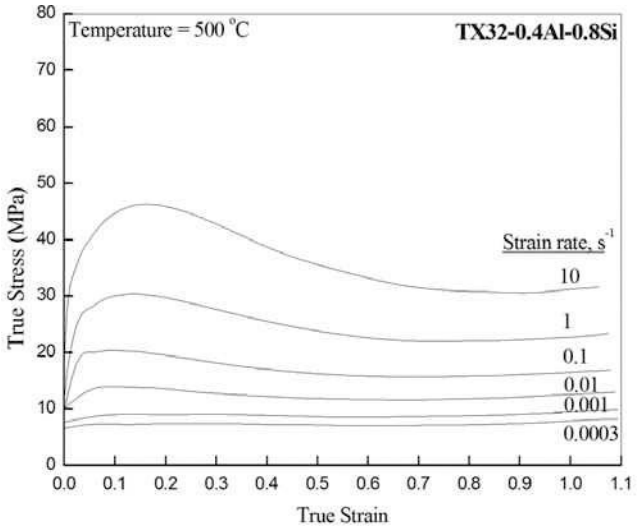

Figure 4. True stress - true strain curves obtained at 500 °C on TX32-0.4Al-0.8Si alloy in compression at different strain rates.

The true stress-true strain curves obtained at the test temperatures of 400 °C and 500 °C are shown in Figure 3 and Figure 4, respectively. At 400 °C and strain rates above 0.1 s^{-1}, the flow stress rapidly increased with increasing strain and reached a peak value before flow softening occurred. At lower strain rates, the flow curves exhibited near steady state deformation. At 500 °C and strain rates lower than 0.01 s^{-1}, the flow curves are of steady-state type from the beginning of deformation. Flow stress decreased significantly with increase in deformation temperature from 400 °C to 500 °C.

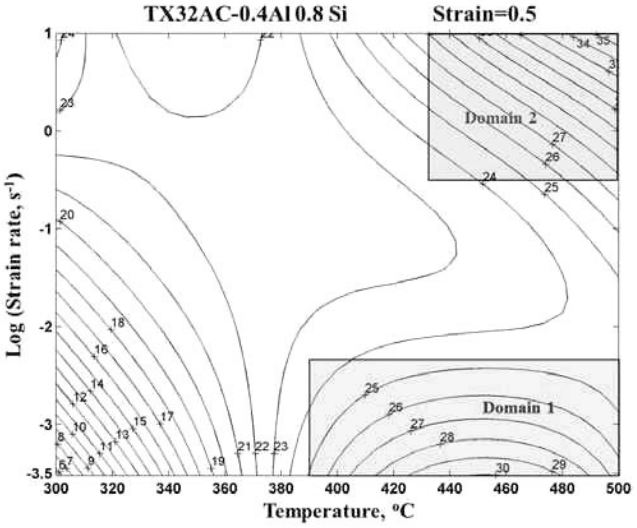

Figure 5. Processing map for TX32-0.4Al-0.8Si alloy. The numbers against the contours represent efficiency of power dissipation in percent.

The processing map obtained at a strain of 0.5 (near steady state flow) is shown in Figure 5. The map exhibits two domains in the temperature and strain rate ranges: (1) 390-500 °C/0.0003-0.005 s^{-1} with a peak efficiency of 30% at 460 °C/0.0003 s^{-1} (Domain 1), and (2) 430-500 °C/0.3-10 s^{-1} with a peak efficiency of 35% at 500 °C/10 s^{-1} (Domain 2). The resultant microstructure of the specimen compressed at 500 °C/10 s^{-1} (Domain 2 peak efficiency condition) is shown in Figure 6 indicate that the alloy undergoes dynamic recrystallization (DRX) during hot working replacing the as-cast microstructure by wrought microstructure.

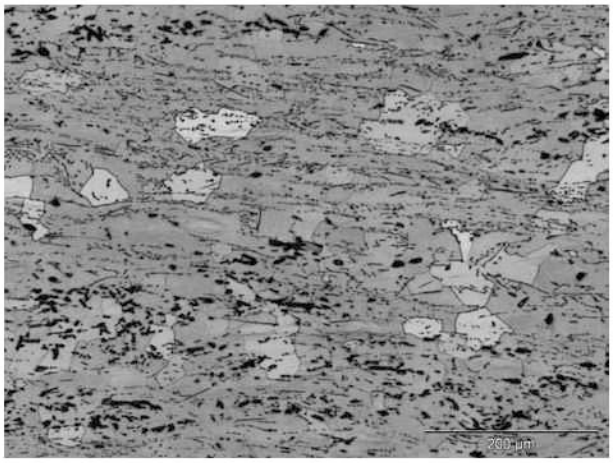

Figure 6. Microstructure of Mg-3Sn-2Ca-0.4Al-0.8Si alloy deformed at 500 °C/10 s^{-1} exhibiting recrystallized grain structure.

It is generally accepted that as-cast alloy exhibit near-random texture. At the start of plastic deformation at lower temperatures (300-350 °C), basal and prismatic slip systems are more likely to operate. When the continued slip on these slip systems causes a rotation of the slip planes towards the normal to the compression axis, favorable slip systems get exhausted and further deformation becomes difficult. This may be the reason for the absence of workability domains at lower temperatures. However, at the deformation temperatures above 400 °C, pyramidal slip systems get activated and contribute to deformation. Also, dynamic restoration processes, like DRX may also occur simultaneously, which help to soften the material. The recovery mechanisms leading to DRX are strain rate dependent; lattice self-diffusion at lower strain rates and grain boundary diffusion at higher strain rates. Thus, while pyramidal slip occurring during DRX cause steady-state flow, two different DRX domains appear in the processing map; one at lower strain rates (0.0003-0.005 s^{-1}) and another at higher strain rates (0.3-10 s^{-1}) at temperature above 430 °C. The stacking fault energy on the second order pyramidal slip systems is reported to be about 173 mJ/m^2 [19] and cross-slip can be the recovery mechanism for nucleating DRX.

Using the standard kinetic rate equation (Eq. 1) to represent the steady-state flow under hot working conditions [20], the activation parameters (stress exponent (n) and apparent activation energy (Q)) are evaluated. A plot of normalized flow stress with strain rate, i.e., ln (σ/μ) vs. ln ($\dot{\varepsilon}$), where μ is shear modulus of Mg is shown in Figure 7. As a single straight line fit over the entire strain rate range is not apparent, the data are separated into two sets of conditions; one for the Domain 1 and another for Domain 2. In the lower strain rate domain (Domain 1), the value of the stress exponent is about 5.88 while it is about 5.68 in the higher strain rate domain (Domain 2).

Arrhenius plot, which relates the normalized flow stress ln (σ/μ) with inverse of temperature, is shown in Figure 8. The data at strain rates of 0.0003 s^{-1} and 0.001 s^{-1} (between 400-500 °C), corresponding to Domain 1 in the processing map, exhibited a linear fit giving an apparent activation energy of 215 kJ/mole. On

the other hand, the data at strain rates of 10 and 1 s^{-1}, i.e., in Domain 2 of the processing map, gave a linear fit only at higher temperatures and yielded apparent activation energy of 175 kJ/mole. The apparent activation energy values obtained for both the domains are much higher than that for self-diffusion in pure magnesium (135 kJ/mole) [20], suggesting that the intermetallic particles in the matrix cause significant back stress. Domain 2 which is occurring at higher strain rates is the recommended window for processing of this alloy as these strain rates can be easily obtained in the commercial deformation processes like rolling and extrusion.

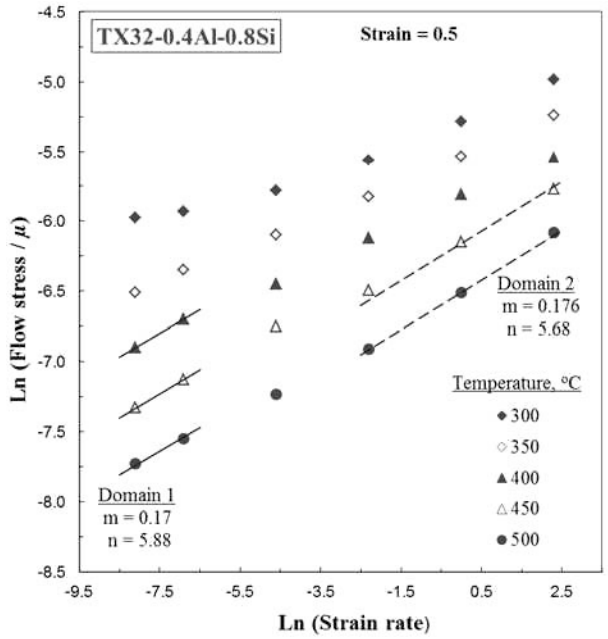

Figure 7. Variation of normalized flow stress values (at a strain of 0.5) with strain rate at different test temperatures for TX32-0.4Al-0.8Si alloy.

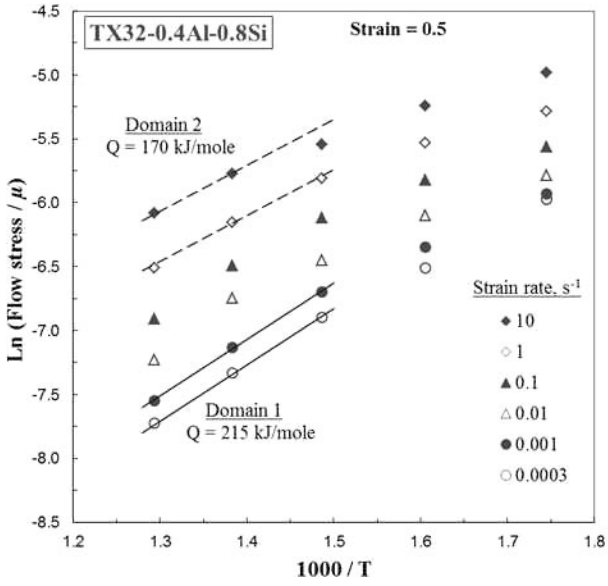

Figure 8. Arrhenius plot showing the variation of normalized flow stress values with inverse of temperature at different strain rates.

Summary and Conclusions

The compressive strength of TX32-0.4Al-0.8Si alloy in as-cast condition in the temperature range 25-250 °C and its hot deformation behavior in the temperature range 300-500 °C and strain rate range 0.0003-10 s^{-1} have been studied using hot compression tests. The flow stress data was used for the kinetic analysis and to develop the processing map for the alloy. The following conclusions are drawn from this study.

(1) Addition of 0.8 wt% Si reduced the compressive strength at all the temperatures.
(2) The stress-strain curves exhibited flow softening after the appearance of a peak stress at high strain rates while near steady-state flow has been observed at lower strain rates.
(3) The processing map exhibited two hot workability domains: (i) 390-500 °C/0.0003-0.005 s^{-1} and (ii) 430-500 °C/0.3-10 s^{-1}, the latter one being suitable for industrial processing.
(4) The apparent activation energy values in the two domains are higher than that for self-diffusion, suggesting the generation of back stress by the intermetallic particles in the matrix.
(5) Dynamic recrystallization is the softening mechanism during hot working of the alloy and is controlled by cross-slip at higher strain rates.

Acknowledgement

This work was supported by a grant (Project #115108) from the Research Grants Council of the Hong Kong Special Administrative Region, China.

References

1. I.J. Polmear, *Metallurgy of the Light Metals*, 3rd edn, Edward Arnold, London, 1995.

2. J.F. Stohr, J.P. Poirier, *Philos. Mag.,* 25 (1972), 1313-1329.

3. F. Kaiser, J. Bohlen, D. Letzig, A. Styczynski, Ch. Hartig, K.U. Kainer, *Mater. Sci. Forum*, 419-422 (2003), 315-320.

4. B.C. Wonsiewicz and W.A. backofen, *Trans. Metall. Soc. AMIE*, 239 (1967), 1422-1431.

5. R.E. Reed-Hill and W.D. Robertson, *Acta Metall.*, 5 (1957), 728-737.

6. S. Suwas, G. Gottstein, R. Kumar, *Mater. Sci. Eng. A*, 471 (2007), 1-14.

7. J.A. Chapman and D.V. Wilson, *J. Inst. Met.*, 91 (1962), 39-40.

8. J. Koike, T. Kobayashi, T. Mukai, H. Watanabe, M. Suzuki, K. Maruyama and K. Higashi, *Acta Mater.*, 51 (7) (2003), 2055-2065.

9. T. Abu Leil, K.P. Rao, N. Hort, Y. Huang, C. Blawert, H. Dieringa and K.U. Kainer, in: *Magnesium Technology 2007*, eds. R.S. Beals, A.A. Luo, N.R. Neelameggham, M.O. Pekguleryuz, TMS (2007), pp.257-262.

10. N. Hort, K.P. Rao, T. Abu Leil, H. Dieringa, Y.V.R.K. Prasad, K.U. Kainer, in: *Magnesium Technology 2008*, eds. M. Pekguleryuz, E. Nyberg, R.S. Beals and N. Neeramegghan, TMS (2008), pp.401-406.

11. K.M. Asl, A. Tari, F. Khomamizadeh, *Mater. Sci. Eng. A*, 523 (2009), 1-6.

12. J.J. Jonas, C.M. Sellars, W.J. McG. Tegart, *Metall. Rev.*, 14 (1969), 1-24.

13. Y.V.R.K. Prasad, T. Seshacharyulu, *Inter. Mater. Rev*, 43 (1998), 243-258.

14. Y.V.R.K. Prasad, S. Sasidhara, *Hot Working Guide: A Compendium of Processing Maps,* Materials Park, Ohio: ASM International; 1997.

15. H. Ziegler, in: I.N. Sneddon, R. Hill (Eds.) *Progress in Solid Mechanics*, Vol. 4, Wiley, New York, (1965), pp. 91-193.

16. Y.V.R.K. Prasad, K.P. Rao. *Mater. Sci. Eng. A*, 374 (2004), 335-341.

17. D.H. kang. S.S. Park, N.J. Kim, *Mater. Sci. Eng. A*, 413-414 (2005), 555-560.

18. M.S. Dargusch, A.L. Bowles, K. Pettersen, P. Bakke, G.L. Dunlop, *Metall. Mater. Trans.*, 35A (2004), 1905-1909.

19. J.R. Morris, J. Schraff, K.M. Ho, D.E. Turner, Y.Y. Ye, M.H. Yoo, *Phil. Mag.*, 76 (1997), 1065-1077.

20. H.J. Frost, M.F. Ashby, *Deformation-mechanism Maps*, (Oxford: Pergamon Press) (1982), p.44.